ANALYSIS OF AU / RHB / HEXANEDITHIOL NANO COMPOSITE SYSTEM

[1]Pooja Patil, [2]Dr. Rakesh Kumar
[1,2]Research Scholar - Chemistry,Shri JJT University, Jhunjhunu, India.

Abstract
Several mercury sensing probes are currently being develop, Due to its robust SPR absorption in the visible range, ease of chemical functionalization, and generally high stability, AuNPs are widely employed for optical sensing applications. AuNPs' SPR absorption is influenced by their size, shape, and refractive index.
Cylindrical forms Triangular-shaped Au NPs have significant IR absorption and strong absorption in the visible range. Aggregation-related AuNP size expansion causes a red shift in the absorbance at longer wavelengths.
Keywords: Chemical functionalization, stability, AuNPs, AuNPs' SPR, size, shape, and refractive index.

1.1. Introduction

Mercury is among the most harmful heavy metal pollutants to human health. It is a naturally occurring element that may be found in “several chemical forms, such as elemental, organic, and inorganic salts. The chemical form of mercury has a significant impact on its toxicity. Methylmercury, dimethylmercury, whereas Hg(II) and Hg(I) salts are accessible inorganic mercury.”

Additionally, depending on the chemical environment, the chemical forms of mercury can alter through interconversion reactions. The most hazardous form of mercury for humans is organic mercury. As a result, mercury in any form is harmful to living things.

Natural processes like coal-burning power plants, oceanic emission, solid waste interaction, etc. have all contributed to the widespread distribution of mercury in the environment. The probable usage of mercury in daily life may be the cause of the environment's rising mercury levels.

The main ways that mercury enters the human body are through water and food Due to mercury buildup in the brain and kidneys, mercury poisoning results in neurological disorders and harms the central nervous system.

Mercury physiologically impacts several brain functions, which can cause symptoms including behavioural abnormalities.

Given that both inorganic and organic mercury ions have extremely harmful effects on living things, including people, quick and precise monitoring of these ions.

Numerous studies are being conducted all around the world to create an analytical probe that is simple, inexpensive.

But these approaches are widespread, labor-intensive, costly, time-consuming, and unsuitable for point-of-use applications. As a result of intensive study on mercury detection during the past 10 years, the colorimetric and fluorescence-based optical approaches are emerging as substitute instruments for mercury detection.

The advantages of functionalized nanoparticles over conventional approaches, such as colorimetry and fluorescence .

Yu et al. “propose a new colorimetric sensor for measuring Hg(II) ions using Au NPs coated with 3-mercaptopropionate acid and adenosine monophosphate. The WHO limit is exceeded by the detection limit for Hg(II) ions, which is 50 ng mL-1. In a separate work, Chen et al. presented a colorimetric assay based on the

coordination of Hg(II) to AuNPs associates 3-nitro-1 H-1,2,4-triazole for the detection of trace quantities of Hg(II) ions (1.4 ng mL-1) in aqueous solution. This assay required costly ingredients and a time-consuming manufacturing process."

The WHO's strict and acceptable limitations make it difficult for researchers to develop a straightforward natural water.

Therefore, a straightforward probe is created in the current study employing AuNPs/RhB/HDT NCS for the very sensitive. Using plasmonic absorbance and fluorescence spectroscopy, the optical characteristics of AuNPs/RhB/HDT NC studied.

Au/RhB/Hexanedithiol Nanocomposite System: An Optical Sensing Probe for Detection of Hg(II) ions in Water

1.2 Preface

Gold nanoparticles (AuNPs)/rhodamine B (RhB)/hexanedithiol (HDT) nanocomposites system (AuNPs/RhB/HDT NCS) has been successfully used to develop a highly selective optical sensing probe for measuring Hg2+ ions in synthetic urine and ground water. RhB is crucial for increasing the sensitivity of Hg (II).

It is crucial to note that the order in which RhB and HDT functionalize AuNPs has a significant impact on the ability to detect Hg(II) ions. RhB was released from AuNPs/RhB/HDT NCS as the basis for the turn-on fluorescence process, which was then used to create the Hg-HDT complex, "whereas the suggested mechanism for Based on the aggregation of composite AuNPs, Hg(II) sensing in absorbance mode.

The linear dynamic range for Hg2+ ion detection using AuNPs/RhB/HDT NCS showed detection limits of 1 ng mL-1 (1 ppb) and 0.5 ng mL-1 (0.5 ppb), respectively. Regarding concentration fluctuation, kinetics, and interference from other metal ions such Na(I), K(I), Mg(II), Ca(II), Fe(III), Co(II), and Ni, the AuNPs/RhB/HDT NCS-based Hg(II) ions detection technique was optimised.(II)."

The examination of linear dynamic range and detection thresholds by both colorimetric and fluorescence systems are covered at the chapter's conclusion. The stability of the AuNPs/RhB/HDT NCS is verified by its longer-than-one-hour absorbance spectrum.\.

1.3 Experimental Details

1.3.1 Synthesis of Au NPs/RhB/HDT nanocomposite system

"The Au NPs were made via citrate-mediated metal reduction in the aqueous phase. Use 25 mL of the deionized water solution for this and 150 L of stock solution of Au (III) ions (12 mM L-1) were combined, held at 85 oC, and next, while continuing to stir the mixture, 0.1 g of trisodium citrate was added." The 0.5 mL citrate-capped Au NPs solution was then mixed with 10 to 50 litres of the 50 mM RhB stock solution prepared in deionized water for 10 minutes.

After the mixture was well incorporated, 2.5–10 L of an ethanol-based HDT (20 pmol L-1) solution was added to the AuNPs/RhB solution while it was being constantly stirred. AuNPs/RhB/HDT nanocomposite system is the name given to the final functionalized Au NPs that were generated.

1.3.2 Hg (II) ion detection in inorganic media

To know "the Hg (II) ion detection reaction mechanism of the AuNPs/RhB/HDT nanocomposite system , controlled experiments have been conducted. Hg(II) (100 mg/L) solution was created by adding 13.5 milligrams of HgCl2 to 100 mL of DI water was created. Standardization By diluting Hg(II) stock solution, optimisation tests for Hg(II) sensing in the concentration range of 5 ng mL-1 to 1000 ng mL-1.

The AuNPs/RhB/HDT solution was added to the analyte solution in a 0.1 mL/0.9 mL ratio for the Hg(II) ion sensing assay and 5 minutes were given for the mixture to stand. The absorbance is used to measure Hg(II) ions."

Ni were optimised for the Au NPs-based Hg(II) ions detection technique.(II). Finally, the improved techniques were used to quantify the Hg(II) ions and urine samples that had been spiked with Hg(II).

1.4 Results and discussion

1.4.1 Structural analysis

XRD pattern verified the production of Au NPs via citrate-mediated reduction. (JCPDF - 04-

0784). The typical diffraction peaks at 2 values 38.2o, 44.35o, 64.75o, and 77.65o This suggests a face-centered cubic (FCC) crystal structure and corresponds to crystal planes (111), (200), (220), and (311), as predicted. Using the Debye-Scherrer formula.

1.4.2 Microscopic analysis

With the use of TEM, the microstructural examination further validated the development of mono- has a 14 nm average particle size, distributed spherical Au NPs. Fig. 3. The (111) plane corresponds to an interplanar gap of 0.23 nm, the high resolution TEM picture of Au NPs demonstrates lattice fringes and validates the crystalline structure of Au NPs. The polycrystalline nature of Au NPs was verified by the diffraction rings that were obtained from the SAED pattern.

The proposed sensing technique was built on the functionalization of citrate-capped Au NPs by RhB and HDT to investigate the detection of Hg(II).

It is important to stress that the precise timing of the addition of RhB and HDT to the citrate-capped Au NPs solution was essential. HDT was added to the citrate-capped Au NPs solution before RhB. As a result, the citrate-capped Au NPs began to combine and their hue abruptly changed from wine red to purple.

The covalent connection cause of the drop in intensity seen at 530 nm, Yu et al. commented on these phenomena in their work, arguing that the significant Au NP aggregations would be connected to the replacement of Au NPs surface.

Citrate ions were shown to be strongly attached to Au NPs in a recent paper by Park and Shumker-Parry, which delays because stabilized network there.

Au NPs are observed aggregation behaviour of Au NPs in the current situation. Because of their strong affinity for Au NPs, organothiol compounds are frequently utilised as stabilising agents. Organothiol compounds bond to au according to the (HSAB) hypothesis.

Metal ion characteristics such as size, charge, polarizability, and electronegativity determine whether they are hard or soft acids. In this instance, HDT is a soft base while Au NPs are a soft acid. According to expectations, thiol terminated HDT molecules should attach to the surfaces of Au NPs and Au ions in a manner similar to that of Au ions by creating an Au-S bond, which results in a self-assembling monolayer. (SAM). When 25 L of 50 M RhB were added to the citrate-capped Au NPs solution before the HDT, there was no appreciable difference, Au NPs solution absorbance spectra with and without RhB and HDT addition.

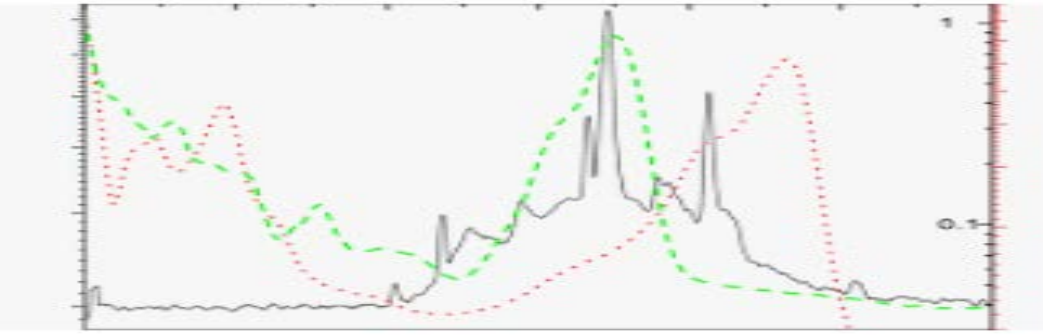

FIGURE 1.1 AU NPS SOLUTION'S ABSORPTION SPECTRA CHANGED AFTER BEING ADDED WITH TOO MUCH RHB.

According to Fig. the considerable rise in RhB peak intensity is detected at 560 nm when RhB (30–50 L of 50 M RhB) is added to the Au NPs solution. As RhB concentration rises.

This is due to too much unreacted RhB, thus in order to prevent it, we have to maximise its concentration in the AuNPs/RhB/HDT NCS. A favourable environment for binding is created by the quarternary amine group present in RhB molecules, which has a unit positive charge, and

the citrate-capped AuNPs' negatively charged surface.

RhB binds to citrate-capped AuNPs primarily through hydrogen bonds and electrostatic interactions. When HDT is introduced to an aqueous solution containing RhB-functionalized, citrate-capped Au NPs, aggregation is not seen. This suggests that the thiol group of HDT binds to a carboxyl group of RhB rather than directly to an Au NP. the potential structural orientation of citrate-capped Au NPs following functionalization with RhB and HDT.

1.5 Optical detection of Hg(II) ions

"The linear regression coefficient R2 = 0.98 and the absorbance spectra in Fig. 1.2 (a-b) unambiguously show that the absorbance peak intensity increases at 660 nm in direct proportion to the amount technique is 1-60 ng mL-1. The detection threshold for the absorbance-based method was 1 ng mL-1.

Table 1.1 compares the present method's detection limit to that of the previously disclosed optical techniques. It clearly suggests that the detection limit achieved in the current case is comparable to other cases that have been reported. The improved sensing technique was finally applied to Hg(II) spiked urine and ground water samples in order to detect Hg(II) ions in the centre of the linear dynamic range for practical use (Fig. 1.2 (b))."

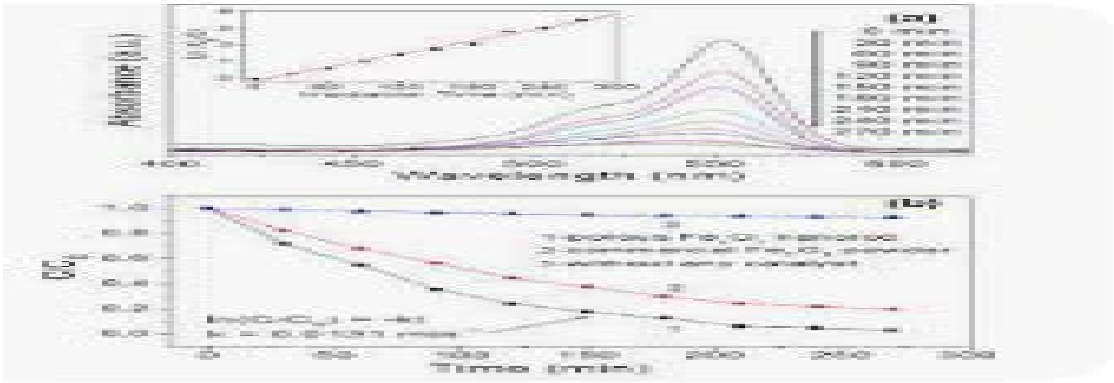

FIGURE 1.2 CHANGE IN AU/RHB/HDT SOLUTION ABSORBANCE INTENSITY AT 670 NM FOLLOWING ADDITION OF VARIOUS CONCENTRATIONS OF HG(II) IONS.

The findings in Table 1.2 unambiguously indicate that the absorbance mode sensing approach successfully recovered 95–98% of the Hg(II).

The continuous efficiency of the ground water and urine samples showed that the complex matrix did not interfere with the recently proposed approach.

Sensing solution for Hg(II) ions	Detection probe	Detection Limit
AuNPs/Peptide	Colorimetric	5 ng mL-1
AuNPs/poly(styrene sulfonate)/ L-ascorbic acid	Colorimetric	5 ng mL-1
AuNPs/polysorbate-80/ L-ascorbic acid	Colorimetric	26 ng mL-1
AuNPs/nitrotriazole	Colorimetric	1.3 ng mL-1

TABLE 1.1 WHEN COMPARED TO CONVENTIONAL OPTICAL APPROACHES BASED ON NP AGGREGATION, "THE DETECTION LIMIT OF THE NEWLY DEVELOPED METHODOLOGY FOR HG(II) SENSING IN AQUEOUS SAMPLES."

Sample ID	(ng mL-1)	Hg(II) detected Mean ± SD	Recovery (%)
	20		97
US-1	30	19.4 ± 0.6	96
US-2	40	28.9 ± 1.0	94
US-3	20	39.2 ± 0.7	93
GWS-1	30	19.1 ± 0.9	94
GWS-2	0	29.2 ± 0.7	98
GWS-3		38.5 ± 0.9	

TABLE 1.2 ANALYSIS OF HG(II) IONS USING AN ABSORBANCE-BASED DETECTION APPROACH IN GROUND WATER AND URINE SAMPLES THAT HAVE BEEN SPIKED WITH HG(II).

The absorption peak at 660 nm suggested an increase in Hg(II) ions' strength.

1.6 Microscopic analysis

Although the Au NPs in the AuNPs/RhB/HDT solution were clearly separated from one another as can be seen in Fig. 1.3. (a), the addition of Hg(II) ions caused an aggregation, as can be observed in Fig. 1.3. (b).

The resultant map and EDS are displayed in Fig. 1.3. (c, d). The surface of the functionalized Au NPs has as seen in the mapping picture, and the presence of both Hg(II) and Au was verified by EDS.

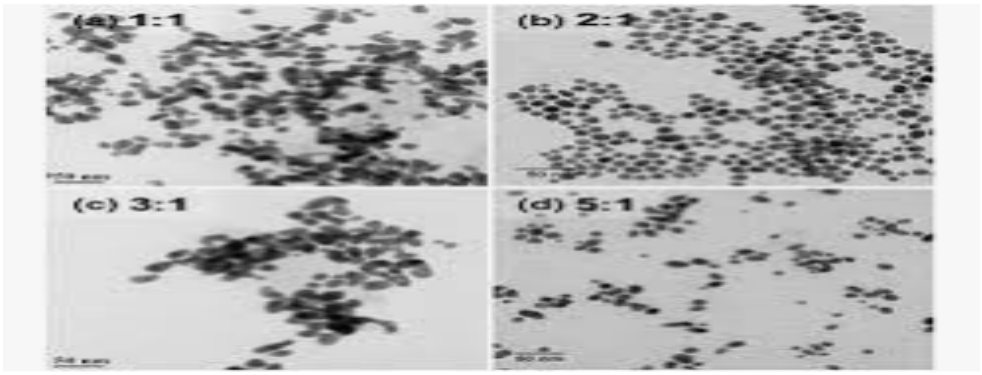

FIGURE 1.3 TEM PICTURES OF THE AUNPS/RHB/HDT AND AFTER ADDING HG(II) IONS, ELEMENTAL MAPPING, AND EDS OF THE AUNPS/RHB/HDT NANOCOMPOSITE.

1.7 Studying the impact of pH and ionic strength on the detection of Hg(II) ions

Ionic strength, pH, and other variables that affect the detecting probe's ability to detect Hg(II) ions was also studied. pH ranges from 3 and 9. Hg(II) ion detection using the AuNPs/RhB/HDT nanocomposite system in an acidic solution. When Hg(II) ions are present at 660 nm, the peck intensity increases in solutions of 1 ng mL-1 and 10 ng mL-1, respectively.

However, a basic pH prevents the AuNPs/RhB/HDT nanocomposite system from detecting the Hg(II) ion in solution. Hg(II) ion detection using the AuNPs/RhB/HDT

nanocomposite system: absorbance spectra in basic pH.

This is so because higher pH values lead to a predominance of metal oxide and metal hydroxide production. Only the Hg(II) ion containing solution exhibits an absorbance peak in the spectrum.

1.8 Selectivity studies

"We also looked into the selectivity of AuNPs/RhB/HDT for Hg(II) ions sensing over other metal ions as Na(I), K(I), Mg, Ca(II), Fe(III), Co(II), and Ni(II). For the examination of individual metal ions, a sample vial containing Hg(II) ions and 1 g mL-1 of metal ions was utilised.

The observed absorbance clearly showed that Na(I), K(I), Mg, Ca(II), Fe(III), and Co had no appreciable effects.(II). In contrast to other metal ions," Ni(II) had a somewhat greater absorbance intensity at 660 nm. The inclusion of HDT in the sensing solution led to a higher selectivity for Hg(II) ions as a result.

1.9. Fluorescence mode for Hg(II) ion detection

AuNPs/RhB/HDT "composite system's "Turn on" fluorescence technique makes it feasible to detect Hg(II) ions using photoluminescence as well. Standardised AuNPs/RhB/HDT nanocomposite system did not show noticeably higher fluorescence when compared to the fluorescence of pure aqueous RhB solution. (In the absence of AuNPs)."

Due to RhB molecules adhering to the surface of AuNPs, RhB and AuNPs are quenched statically by a non-Forster FRET. Stobiecka and Hepel also said that electrostatic and hydrogen bonding are both interactions between RhB and citrate-capped AuNPs. The amount of Hg(II) ions in the solution increased in direct proportion to the fluorescence intensity of the mixture.

As a result of Hg(II) the RhB molecules would be displaced into the solution. The current "Turn on fluorescence technique demonstrated a dynamic linear range in the concentration range of 0.5 - 40 ng mL-1 of Hg(II) ions in aqueous samples with regression value of R2 = 0.971." The detection threshold for the fluorescent mode technique is 0.5 ng mL-1.

1.10 Reproducibility Studies

The AuNPs/RhB/HDT nanocomposite system's repeatability for the detection of Hg(II) ions was successfully tested at least three times.

1.11 Stability studies

AuNPs/RhB/HDT is confirmed by absorbance spectra to be more than one hour. The Fig. 9.22 contained absorbance spectra taken for freshly prepared AuNPs/RhB/HDT nanocomposite solution and after one hour. It shows same spectra for both samples, initial and after one hour confirmed good stability of solution.

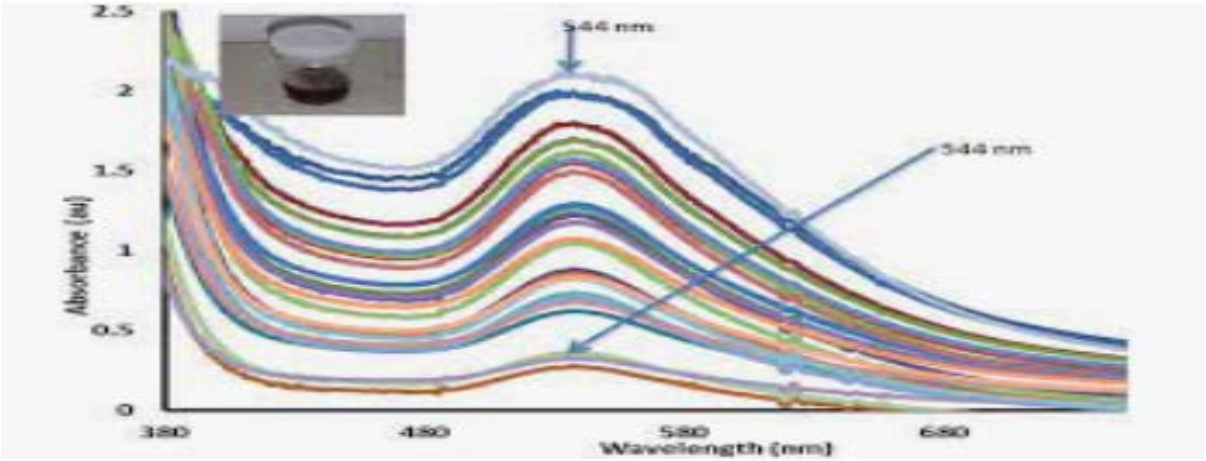

FIGURE 1 .4 STABILITY OF AUNPS/RHB/HDT NANOCOMPOSITE SYSTEM BY ABSORBANCE SPECTRA

1.12 Conclusion

Aggregation of functionalized AuNPs was used to find Hg(II). HDT was added to provide the present method the necessary selectivity for Hg(II) ions.

By using spectrophotometry, it was discovered that the method's dynamic range was 1- 60 ng mL-1. Additionally, the currently employed "Turn on fluorescence approach demonstrated a greater dynamic linear range in the concentration range of 0.5 - 40 ng mL-1 Hg(II) ions in aqueous samples with a 0.5 ng mL-1 detection limit."

The method's detection limit exceeded the WHO's allowable limit for drinking water. The artificial ground water and urine samples were successfully used to test the effectiveness of the optimised absorbance-based approach.

References

1. Aawani, E., Memarian, N., and Dizaji, H. R. Synthesis and characterization of reduced graphene oxide–V2O5 nanocomposite for enhanced photocatalytic activity under different types of irradiation. Journal of Physics and Chemistry of Solids, 125:8-15, 2019.
2. Abhilash, M. R., Akshatha, G., and Srikantaswamy, S. Photocatalytic dye degradation and biological activities of the Fe2O3/Cu2O nanocomposite. RSC Advances, 9(15):8557-8568, 2019.
3. Alirezvani, Z., Dekamin, M. G., and Valiey, E. Cu(II) and magnetite nanoparticles decorated melamine-functionalized chitosan: A synergistic multifunctional catalyst for sustainable cascade oxidation of benzyl alcohols/Knoevenagel condensation. Scientific Reports, 9(1):1-12, 2019.
4. An, C., Zhang, Y., Guo, H., and Wang, Y. Metal oxide-based supercapacitors: Progress and prospectives. Nanoscale Advances, 1:4644-4658, 2019.
5. Ayogu, J. I. and Onoabedje, E. A. Recent advances in transition metal-catalysed cross-coupling of (hetero)aryl halides and analogues under ligand-free conditions. Catalysis Science & Technology, 9(19):5233-5255, 2019.
6. Biraj Das , Nanostructured Metallovanadates of Silver and Gold: Synthesis, Characterization and their Application as Environmental Catalyst , at shodganga.com ,jan,2020.
7. Chakraborty, A., Chakraborty, T., Menendez, M. I., and Chattopadhyay, T. Surfactant-mediated solubilization of magnetically separable nanocatalysts for the oxidation of alcohols. ACS omega, 4(7):11558-11565, 2019.
8. Chakraborty, T., Chakraborty, A., Maity, S., Das, D., and Chattopadhyay, T. Conglomerated system of Ag nanoparticles decorated Al2O3 supported cobalt and copper complexes with enhanced catalytic activity for oxidation reactions. Molecular Catalysis, 462:104-113, 2019.
9. Chen, D., Xie, Q., and Zhu, J. Unconventional aromaticity in organometallics: The power of transition metals. Accounts of Chemical Research, 52(5):1449-1460, 2019.
10. Craig, M. J., Coulter, G., Dolan, E., Soriano-López, J., Mates-Torres, E., Schmitt, W., and García-Melchor, M. Universal scaling relations for the rational design of molecular water oxidation catalysts with near-zero overpotential. Nature Communications, 10(1):1-9, 2019.
11. Das, R., Sypu, V. S., Paumo, H. K., Bhaumik, M., Maharaj, V., and Maity, A. Silver decorated magnetic nanocomposite (Fe3O4@PPy-MAA/Ag) as highly active catalyst towards reduction of 4-nitrophenol and toxic organic dyes. Applied Catalysis B: Environmental, 244:546-558, 2019.
12. Dong, X. Y., Zhang, Y. F., Ma, C. L., Gu, Q. S., Wang, F. L., Li, Z. L., Jiang, S. P., and Liu, X. Y. A general asymmetric copper-catalysedSonogashira C(sp3)–C(sp) coupling. Nature Chemistry, 11(12):1158-1166, 2019.
13. Dowling, A. P. Development of nanotechnologies. Materials Today, 7(12):30-35, 2004.
14. Du, M., Zeng, G., Huang, J., Sun, D., Li, Q., Wang, G., and Li, X. Green photocatalytic oxidation of benzyl

alcohol over noble-metalmodified H2Ti3O7 nanowires. ACS Sustainable Chemistry & Engineering, 7:9717−9726, 2019.

15. Endrődi, B., mulders, V., imic, N., Wildlock, M., Mul, G., Mei, B., and Cornell, A. In situ formed vanadium-oxide cathode coatings for selective hydrogen production. Applied Catalysis B: Environmental, 244:233-239, 2019.
16. Fujita, T., Fuchibe, K., and Ichikawa, J. Transition-metal-mediated and-catalyzed C−F bond activation by fluorine elimination. Angewandte Chemie International Edition, 58(2):390-402, 2019.
17. Ganguly, P., Harb, M., Cao, Z., Cavallo, L., Breen, A., Dervin, S., Dionysiou, D. D., and Pillai, S. C. 2D nanomaterials for photocatalytic hydrogen production. ACS Energy Letters, 4(7):1687-1709, 2019.
18. Huo, D., Kim, M. J., Lyu, Z., Shi, Y., Wiley, B. J., and Xia, Y. One-dimensional metal nanostructures: From colloidal syntheses to applications. Chemical Reviews, 119(15):8972-9073, 2019.
19. Jung, J. S. and Kim, S. H. Application of smectite for textile dyeing and fastness improvement. RSC Advances, 9(63):36631-36639, 2019.
20. Kaboudin, B., Saghatchi, F., and Kazemi, F. Synthesis of decorated carbon nanotubes with Fe3O4 and Au nanoparticles and their application in catalytic oxidation of alcohols in water. Journal of Organometallic Chemistry, 882:64-69, 2019.
21. K. DATTATRAY DAWARE in SILICA-METAL CORE-SHELL NANOSTRUCTURES; (SiO2@Au, SIO2@Pt, SIO2@Pd): SYNTHESIS, CHARACTERIZATION AND ITS ENVIRONMENTAL APPLICATIONS. Shodganga.com.in 2020
22. Lee, K., Yoon, H., Ahn, C., Park, J., and Jeon, S. Strategies to improve the photocatalytic activity of TiO2: 3D nanostructuring and heterostructuring with graphitic carbon nanomaterials. Nanoscale, 11(15):7025-7040, 2019.
23. Lou, S., Wang, W., Wang, L., and Zhou, S. In-situ oxidation synthesis of Cu2O/Ag/AgCl microcubes with enhanced visible-light photocatalytic activity. Journal of Alloys and Compounds, 781:508-514, 2019.
24. Luo, C., Fu, F., Yang, X., Wei, J., Wang, C., Zhu, J., Huang, D., Astruc, D., and Zhao, P. Highly efficient and selective Co@ZIF-8 nanocatalyst for hydrogen release from sodium borohydride hydrolysis. ChemCatChem, 11(6):1643-1649, 2019.
25. Manrique, E., Ferrer, I., Lu, C., Fontrodona, X., Rodríguez, M., and Romero, I. A heterogeneous ruthenium dmso complex supported onto silica particles as a recyclable catalyst for the efficient hydration of nitriles in aqueous medium. Inorganic Chemistry. 58:8460-8470, 2019.
26. Mera, G., Kroll, P., Ponomarev, I., Chen, J., Morita, K., Liesegang, M., Ionescu, E., and Navrotsky, A. Metal-catalyst-free access to multiwall carbon nanotubes/silica nanocomposites (MWCNT/SiO2) from a single-source precursor. Dalton Transactions, 48:11018-11033, 2019.
27. Moradi, M., Moussavi, G., Yaghmaeian, K., Yazdanbakhsh, A., Srivastava, V., and Sillanpää, M. Synthesis of novel Ag-doped S-MgO nanosphere as an efficient UVA/LED-activated photocatalyst for non-radical oxidation of diclofenac: Catalyst preparation and characterization and photocatalytic mechanistic evaluation. Applied Catalysis B: Environmental, 260:118128, 2020.
28. Pembere, A. M., Cui, C., Anumula, R., Wu, H., An, P., Liang, T., and Luo, Z. A hexagonal Ni6 cluster protected by 2-phenylethanethiol for catalytic conversion of toluene to benzaldehyde. Physical Chemistry Chemical Physics, 21(32):17933-17938, 2019.
29. Rayati, S., Pournaser, N., Nejabat, F., and Nafarieh, P. Aerobic oxidation of cyclohexene over Mn-porphyrin based nanocatalyst: Supported vs unsupported catalyst. Inorganic Chemistry Communications, 107:107447, 2019.

30. Tang, C., Zhang, N., Shao, Q., Huang, X., and Xiao, X. Rational design of ordered Pd–Pb nanocubes as highly active, selective and durable catalysts for solvent-free benzyl alcohol oxidation. Nanoscale, 11(12):5145-5150, 2019.
31. Wei, Q., Liu, T., Wang, Y., and Dai, L. Three-dimensional N-doped graphene aerogel-supported Pd nanoparticles as efficient catalysts for solvent-free oxidation of benzyl alcohol. RSC Advances, 9(17):9620-9628, 2019.
32. Zhu, Y., Liu, X., Jin, S., Chen, H., Lee, W., Liu, M., and Chen, Y. Anionic defect engineering of transition metal oxides for oxygen reduction and evolution reactions. Journal of Materials Chemistry A, 7(11):5875-5897, 2019.